Energy 226 (2021) 120364

Contents lists available at ScienceDirect

Energy

journal homepage: www.elsevier.com/locate/energy

Long-term changes in offshore wind power density and wind turbine capacity factor in the Iberian Peninsula (1900–2010)

Sheila Carreno-Madinabeitia [a, *], Gabriel Ibarra-Berastegi [b, e], Jon Sáenz [c, e], Alain Ulazia [d]

[a] Faculty of Pharmacy, Department of Mathematics, University of the Basque Country (UPV-EHU), Vitoria-Gasteiz, Spain
[b] Faculty of Engineering, Energy Engineering Department, University of the Basque Country (UPV-EHU), Bilbao, Spain
[c] Faculty of Science and Technology, Department of Physics, University of the Basque Country (UPV-EHU), Leioa, Spain
[d] Faculty of Engineering, Energy Engineering Department, University of the Basque Country (UPV-EHU), Eibar, Spain
[e] Plentziako Itsas Estazioa (BEGIK), University of the Basque Country (UPV-EHU), Plentzia, Spain

ARTICLE INFO

Article history:
Received 2 September 2020
Received in revised form
20 January 2021
Accepted 9 March 2021
Available online 15 March 2021

Keywords:
Offshore wind power density
Capacity factor
Trends
ERA5
ERA-20C
20th century
Fluid mechanics

ABSTRACT

This study analysed temporal and spatial changes in offshore wind power density (WPD) and capacity factor (CF) around the Iberian Peninsula during the 20th century by analysing data from ERA20 and ERA5. Both WPD and CF were calculated using reanalysis data considering a wind turbine with a hub height of 90 m and incorporating the effect of air density changes. Since ERA5 assimilates more observations, the data from ERA20 was bias-corrected using quantile matching, with ERA5 reanalysis data as the reference. As both variables are based on wind speed (WS), this variable was also corrected and analysed. The results show that the mean values for WPD, CF, and WS during the 20th century were highest in the Atlantic zone and the Gulf of Lyon and lowest around the Balearic Islands. The results of the assessment of decadal trends using the Theil–Sen estimator show that all indicators increased significantly in the waters of the Iberian Peninsula during the study period (1900–2010). Considering the mean slope over this period, the change over the entire period could amount to 174 Wm^{-2} for WPD, 8.8% for CF, and 1.1 ms^{-1} for WS. Based on these changes, offshore wind turbines would have increased their returns by approximately 20% over the 11 decades.

1. Introduction

In recent years, there has been growing interest in renewable energy as a means to mitigate the negative effects of climate change. Liu et al. [1] demonstrated a direct association between renewable energy consumption and reductions in CO_2 emissions in multiple countries (Brazil, India, China, and South Africa).

Worldwide, wind power is the second leading source of renewable energy after hydroelectric power. These sources generate 591 and 1132 GW per year, respectively, according to the Renewables Global Status Report in 2019 [2]. This report indicates that Spain is among the five countries with the greatest installed wind power capacity worldwide. Moreover, Spain and Portugal are above the third quantile in the European Union (EU) in terms of installed wind power capacity [3]. These data are in line with those published by the International Renewable Energy Agency [4], which are summarised in Table 1. It also shows how the installed wind power capacity is expected to increase by 2030 according to the EU Directorate-General for Energy [5] and National Renewable Energy Action Plans of Spain [6] and Portugal [7].

The EU is committed to the development of offshore wind power in the long term. It is the region with the highest floating wind energy capacity, approximately 77% (Table 1) of the global total. The EU Directorate-General for Energy forecasts that this technology will contribute the most to the increase in renewable power proposed for the near future. This is in line with the offshore wind strategy in the European Green Deal [8], marking the first steps towards a more sustainable economy in the EU. In Europe, offshore wind power is focused in the North Sea, supported through the North Seas Energy Cooperation [9]. Recently, however, attention has been focused on the Mediterranean Sea and Atlantic Coast.

The most widely used indicators for measuring wind energy potential are wind power density (WPD) [10] and capacity factor (CF) [11], which, in the literature, are customarily derived from wind speed (WS). The former is used for wind resource assessments of an area under study, while the CF for a given wind turbine

* Corresponding author.
E-mail address: Sheila.Carreno@ehu.eus (S. Carreno-Madinabeitia).

https://doi.org/10.1016/j.energy.2021.120364

Table 1
Present and future installed wind power capacity (GW).

	2019		2020	2030
	Onshore GW (%)	Offshore GW (%)	GW	GW
World	594.4 (100)	20.31 (100)		
Europe	173.95 (29.26)	21.83 (77.12)	210	350
Spain	25.55 (4.30)	0.05 (0.02)	28.03	50.33
Portugal	5.23 (0.88)	0.08 (0.03)	5.4	9.2

at a specific location is an indicator of actual power generation with respect to the nominal power. According to a European study [12], the mean CF for European wind turbines assessed in 2018 was 24%, rising to 37% when considering only offshore wind power. Notably, the Hywind Scotland pilot park, an offshore floating wind farm, has achieved a CF of 53.8% [13]. Both WPD and CF should be calculated by combining site-specific air density and wind speed data. However, few studies have considered the impact of changes in air density [14,15] on WPD. Considering the 1950–2010 period in the Northern Hemisphere [16], oscillations of approximately 6% in WPD can be attributed to air density changes alone. Specifically, for the Iberian Peninsula (IP), during the 2009–2014 period, the variation may reach 8% in the case of WPD and 1% for CF [17].

In recent years, numerous studies have been published on offshore wind power, and their main objective has been to analyse the wind power potential of many sites across the world that are markedly different from each other. For example, for Africa [18], Blended Sea Winds (BSW) [19] datasets from satellite observations over 11 years were used to analyse wind resources and CFs in two scenarios, one near the coast and the other in deep waters. In Colombia, WS and WPD were investigated for the 1979–2015 period [20] using North American Regional Reanalysis data [21]. WPD analysis has also been carried out at specific sites in Kuwait [22]. In the northeast of Scotland [15], estimates of WPD and CF have been obtained using ERA5 [23] reanalysis data for the 2008–2017 period. Several studies have also been conducted in the waters around the IP. The WPD in the Mediterranean Sea was analysed [24] based on BSW datasets from the National Oceanic and Atmospheric Administration (NOAA) for a 20-year period (1995–2014). Salvação et al. [25] used the 6-hourly output of the Weather Research and Forecasting (WRF) model [26] to calculate WPD and CF offshore the IP during 2004–2013. All of these studies provide an average or static picture of the current WPD and CF, using at most 37 [20] years of data. In these works, long-term changes and the effects of air density have not been considered.

To date, most studies analysing changes in offshore wind power have used WPD based on WS data to make future projections. These studies typically focus on analysing the impact of climate change, with an underlying interest in economic analysis, as future changes in the available resources will also require changes in the management of wind farms already in operation. Specifically, Zheng et al. [27] used observations obtained between 1980 and 1999 as a reference to analyse the future projections of worldwide WPD from the Coupled Model Intercomparison Project 5 (CMIP5) [28], considering the low and medium climate change scenarios (Representative Concentration Pathways [RCPs] 2.6 and 4.5). Costoya et al. [29] performed a similar analysis for the western part of the IP, considering the years 2025–2100, with the worst-case scenario (RCP 8.5). Another study carried out in the Mediterranean Sea [30] analysed an intermediate scenario (RCP 4.5) considering both 1976–2005 and 2021–2050 periods.

To demonstrate the capability of climate projections combined with operational tools for offshore wind farm planning, the European Centre for Medium-Range Weather Forecasts (ECMWF) undertook a project that consisted of simulations of seven wind farms in Northern Europe using the projections of the HIRHAM5/EC-EARTH model with RCPs 4.5 and 8.5 as input [31]. This was the first study to explore the effect of climate change on the operation and maintenance of floating wind farms. The results obtained [32] concerning the energy generated suggested a 3% reduction (RCP 8.5) and a 2% reduction in mean WS (RCP 4.5 and 8.5). As this study only considered one model and two climate scenarios, there is a need for further research in this field.

To the best of the author's knowledge, no studies have investigated long-term changes in WPD or CF during the 20th century. However, analyses were carried out for other variables, such as wave energy [33,34], daily precipitation [35], WS [36] and ocean WS and wave height [37,38].

Previous studies have generally estimated WPD and CF using reanalysis data. ERA5 reanalysis has been widely used to analyse wind in specific regions. Jourdier [39], using ERA5 and other reanalyses such as NASA's MERRA2 and COSMO-REA6 from the German Weather Service (DWD), concluded that ERA5 provides good results with a low bias for WS in the northern half of France. In Brazil, De Assis Tavares et al. [40] validated WS from the CFSv2, ERA5, and MERRA2 reanalyses at five buoys, concluding that ERA5 yielded the best results. With the same objective and results, Olauson [41] compared ERA5 with MERRA2 for the specific case of wind power for 1051 wind turbines in five countries: Germany, Denmark, France, Sweden, and the USA (Bonneville). One of the conclusions of this work was that ERA5 data can be used to accurately estimate the wind power potential. This database was also used to calculate WPD and CF in another region close to the IP, namely, the northeast of Scotland [15].

According to Wohland et al. [42], in long-term assessments, it is necessary to complement the current reanalysis ERA5, with long-term reanalysis datasets such as ERA-20C [37] or 20CR [36,43]. These long-term reanalyses (ERA-20C and 20CR) provide estimations of the state of the atmosphere through longer periods, albeit with a coarser spatial resolution and less assimilated observations than reanalyses such as ERA5. ERA20-C has been selected because it is widely used in studies that analyse trends over the 20th century [33–35].

Nonetheless, these long-term reanalyses require careful recalibration [44–47] with current reanalysis datasets (e.g. ERA5), which cover a shorter timespan (approximately 40 years). These modern reanalyses are better constrained by observations as they assimilate other types of data that are not used by the assimilation model in ERA-20C, such as satellite radiance data, vertical soundings, and surface observations. For this reason, to extend the study back to 1900, it is necessary to calibrate 20th century data by combining information from the two above-mentioned reanalyses in their overlapping period.

The objectives of this study are as follows:

1. To analyse long-term changes in offshore WPD and CF over 111 years (1900–2010) in the waters around the IP.
2. To characterise both the spatial structure and the low-frequency time variations of three variables (WPD, CF, and WS).
3. To classify the area of study into subareas according to its wind power potential as defined by the average WPD.

For all three objectives, the effect of air density oscillations needed to be incorporated into the calculations. As a reference, the National Renewable Energy Laboratory's (NREL) 5-MW turbine [48], FAST 5 MW, with 126 m diameter and 90 m hub height was selected.

The paper is divided as follows: Section 2 presents the datasets and the methods used in this study. Section 3 describes the results,

Section 4 discusses the results, and Section 5 concludes this study and outlines areas for future work.

2. Data and methods

2.1. Data

In this study, offshore WPD, CF, and WS around the IP were analysed, specifically for the region from 15° W to 10° E and 32.5°—to 50 °N, as shown in Fig. 1. To calculate and validate the results of WPD, CF, and WS over the 20th century, two sources of data were used: the ECMWF 20th century reanalysis, ERA-20C (ERA20 hereafter), and ERA5 reanalysis.

ERA20 is based on data from 1900 to 2010 and has a spatial resolution of 1.5° × 1.5°. The variables used for calculating both WPD and CF are as follows:

- 10 m zonal wind component (U_{10})
- 10 m meridional wind component (V_{10})
- 100 m zonal wind component (U_{100})
- 100 m meridional wind component (V_{100})
- 2 m temperature (T_2)
- 2 m dewpoint temperature (d_2)
- Atmospheric sea level pressure (mslp)

The temporal resolution of these variables ranges between 3 and 6 h, and for this study, the resolution was taken as 6 h in all cases, as only 6-hourly data are available for temperature.

To combine ERA20 data with ERA5, ERA5 data corresponding to the same set of variables were downloaded at the same spatial and temporal resolution. For this study, an ERA5 land—sea mask was used to identify the grid points over the sea (Fig. 1).

2.2. Methods

2.2.1. Calculation of WS, WPD, and CF

In this study, a 90-m high turbine was selected, and hence, the first step was to calculate the WS at that hub height. This is the height of the hub of the National Renewable Energy Laboratory's 5-MW offshore turbine [48] which was used as a reference. WS at 10 and 100 m were calculated using zonal and meridional components at those heights according to Equations (1) and (2).

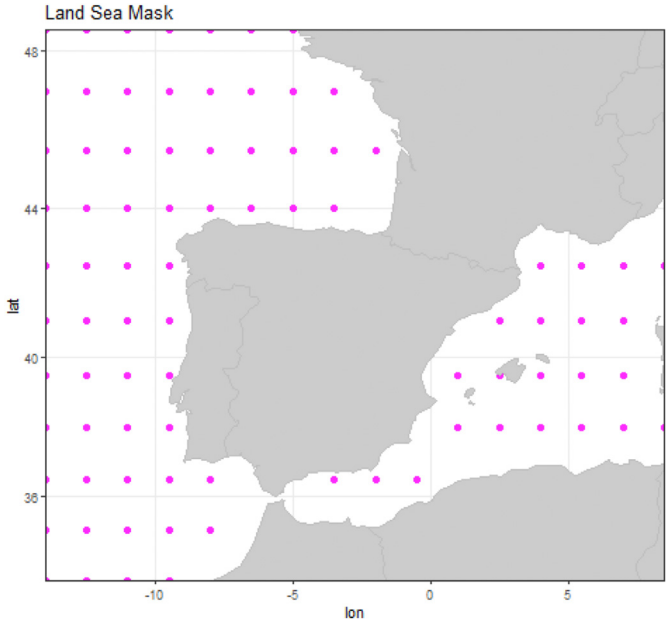

Fig. 1. Masks used by ERA5 and ERA20, the magenta dots indicating points identified as water.

$$WS_{10} = \left(U_{10}^2 + V_{10}^2\right)^{1/2} \tag{1}$$

$$WS_{100} = \left(U_{100}^2 + V_{100}^2\right)^{1/2} \tag{2}$$

As WS changes logarithmically with height, sea surface roughness z_0 was calculated from WS at 10 and 100 m, for each grid point at 6 h intervals according to Equation (3). Then, WS at 90 m was calculated by applying Equation (4).

$$\frac{WS_{100}}{WS_{10}(10)} = \frac{\log\left(\frac{100}{z_0}\right)}{\log\left(\frac{10}{z_0}\right)} \tag{3}$$

$$WS_{90}(90) = WS_{10}(10)\frac{\log\left(\frac{90}{z_0}\right)}{\log\left(\frac{10}{z_0}\right)} \tag{4}$$

The second variable of interest in this study was WPD, an indicator of the wind energy available at a given site and height. Specifically, it is the power available per square meter of area normal to the incoming wind (Equation (5)). This calculation includes both WS at 90 m and air density (ρ) [10].

$$WPD = \frac{1}{2}\rho(WS_{90})^3 \tag{5}$$

The other variable of interest, CF, indicates the energy produced by turbines with respect to what would be produced if turbines were operating at their rated power (P_R). CF is widely used to measure the average load of power plants such as wind farms [12,49,50] and solar photovoltaic arrays [51,52]. It can be used to compare different plants and technologies [53]. To calculate the CF of a commercial turbine, first, WS was normalised (WS_n). Using air density (Equation (6)), the CF was calculated using Equation (7) [11]. In this estimation, many reference turbines with rated power of approximately 1 and 2 MW [11] have been used. The authors have already demonstrated the accuracy of Equation (7) for turbines that are larger (with longer and wider blades) and taller [15,54,55], such as the aforementioned NREL 90-m 5 MW turbine. In the previous articles, the CF relative error for a 5 MW turbine was less than 5% if the CF was calculated using the power curve procedure instead of calculating it with Equation (7). Additionally, the remainder terms in the equation that accounts for the turbine characteristics (P_R and D) are not relevant when the absolute difference in CF as a percentage has been calculated. Only the hub height makes a difference.

$$WS_n = WS\left(\frac{\rho}{\rho_0}\right)^{\frac{1}{3}} \tag{6}$$

$$CF = 0.087\ WS_n - \frac{P_R}{D^2} \tag{7}$$

where P_R is the rated power of the turbine in kW and D is the diameter in meters.

The accurate calculation of the WPD and normalised WS involves the previously calculated air density. As mentioned above,

although air density is customarily considered to be constant in most studies, $\rho_0 = 1.225$ kg/m^3, it can be accurately calculated if pressure, temperature, and humidity information are known. As ERA5 and ERA20 data include atmospheric pressure at sea level (mslp) and 2 m and dewpoint temperatures (T_2 and d_2), the air density at each grid point was calculated to obtain better results for WPD and CF. Details on performing these calculations using T_2, d_2, and mslp with the R package *aiRthermo* [56] can be found in the work of Ibarra-Berastegi et al. [14].

2.2.2. Adjustment of reanalysis data

The 20th century ERA20 reanalysis assimilates fewer observations than more recent reanalyses, such as ERA5. Therefore, the adjustment of ERA20C data using ERA5 aims to transfer the additional information available in ERA5 to ERA20. For the calibration process, the quantile matching technique was used, which involves calculating the percentiles of ERA20 data to be corrected, and the percentiles of ERA5 data for the common years in which data are available from both reanalyses (1979–2010). In this way, the relatively more recent ERA5 reanalysis that incorporates more detailed information can be used to correct biases in the ERA20 reanalysis, which covers a longer period, thus obtaining an adjusted ERA20 reanalysis (ERA20adj).

This approach is a widely used method for bias correction with the aim of achieving various goals, such as the adjustment and homogenisation of climate data series [57,58], or as in this study, the correction of biases in 20th century reanalysis using more recent reanalysis for a shorter period (in this case, 32 years). This methodology has been previously applied for different target variables such as WS [36] and wave energy resources [33,34]. For this purpose, Gudmundsson et al. [59] indicate that non-parametric transformations perform better than parametric transformations or those based directly on the distribution. Among possible non-parametric techniques, quantile matching seems to outperform statistical smoothing spline methods. The success of the non-parametric approach is likely due to its flexibility and as it does not depend on a preset function. The aforementioned authors also indicate that non-parametric methods are, on average, better able to reduce systematic errors, even in the case of the highest percentiles (the extremes).

In this study, the variables of interest are WPD, CF, and WS, which were calculated from the information available in the reanalysis. Considering that the relationships of WPD and CF with air density and WS are nonlinear, the best approach to reduce the final errors was to directly calibrate WPD and CF.

2.2.3. Calculation of mean data and decadal changes

First, mean values at each grid point based on 6-hourly WPD, CF, and WS data from the whole period were computed. Maps with three variables were produced for different seasons, considering December to February to be winter; March to May, spring; June to August, summer; and September to November, autumn. The spatial mean of the variables in the map were also shown on all maps over land.

To calculate long-term changes, WPD, CF, and WS monthly data were used. To reduce the interference of seasonal variations in the variables, anomalies were identified for the whole period (1900–2010). A 30 year reference period (1981–2010) was used to compute the seasonal cycle, and the anomalies were identified by subtracting the seasonal cycle from the original data at each grid point.

Box plots were used to graphically represent the variability of WPD, CF, and WS over time. To build the box plot for each decade, the corresponding monthly anomalies of each grid point were used.

Table 2
WPD classifications categories at 90 m.

Categories	$WPD_{90\ m}$ (Wm^{-2})	$WS_{90\ m}$ (ms^{-1})
1. High	>1050	>9.8
2. Medium-high	(640, 1050]	(8.4, 9.8]
3. Medium	(440, 640]	(7.4, 8.4]
4. Medium-low	(240, 440]	(5.9, 7.4]
5. Low	≤240	≤5.9

Together with the box plots, the trends from the decadal median were calculated using the Theil–Sen estimator [60,61] from monthly anomalies. This method is much more robust than a simple linear regression, as it calculates the mean of the slopes between all possible pairs of points. For this reason, it can reduce the influence of extreme values and allows the calculation of 95% confidence intervals.

2.2.4. Classification of areas by WPD values

According to classical ranges used in wind energy, WPD classification maps were generated according to the usual division into five major wind energy potential categories [62]. To that end, the WPD at 90 m height was calculated (Table 2) for all grid points in the studied area. The procedure to perform the classification was as follows: first, the annual mean values of WPD and WS at each grid point were calculated; next, considering Table 2, the categories were selected; and finally, the mean category for the entire period was calculated.

3. Results

3.1. Calibration of ERA20adj data

The panels in Fig. 2 show the results for each reanalysis for the overlapping period (1979–2010) in the three datasets (ERA20, ERA5, and ERA20adj).

The differences in WPD, CF, and WS between ERA5 and ERA20 were as large as 648 Wm^{-2}, 0.24, and 2.8 ms^{-1}, respectively (not shown). The greatest differences between these datasets are found at the points closest to the coast and in the Mediterranean Sea. As expected, because of adjusting ERA20 data using ERA5, the resulting dataset (ERA20adj) shows the same patterns of high WPD, CFs, and WSs as in ERA5, particularly in the Mediterranean Sea and in the northwest of the study area.

3.2. Spatial means

Considering the WPD and CF mean values in ERA20adj data for the entire period 1900–2010 (Fig. 3), interesting zones with high WPD values (above 600 Wm^{-2}) can be observed. In particular, in the Atlantic, including around A Coruña and along the French coast, as well as the Gulf of Lyon in the Mediterranean Sea. The region around Cabo de Gata should also be highlighted, as the mean WPD there is as high as 590 Wm^{-2}. Note that the areas with the highest WPDs also have the highest CFs (WSs), with values above 0.4 (8 ms^{-1}) being found in the northwest of the study area. Around the Gulf of Lyon, values between 0.35 and 0.48 (between 7.1 and 9.1 ms^{-1}) have been estimated, and 0.37 (7.8 ms^{-1}) was estimated around Cabo de Gata (Fig. 3). Based on the overall mean values of WPD and WS for the whole period, a classification of grid points was carried out by wind energy potential (Table 2), thus identifying five major regions in the study area. The most energetic areas are located NW of the Iberian Peninsula and in the Gulf of Lyon (Figs. 3 and 4), while the WPD tends to decrease near the coast of the IP.

The behaviour of the study variables WPD, CF, and WS differed

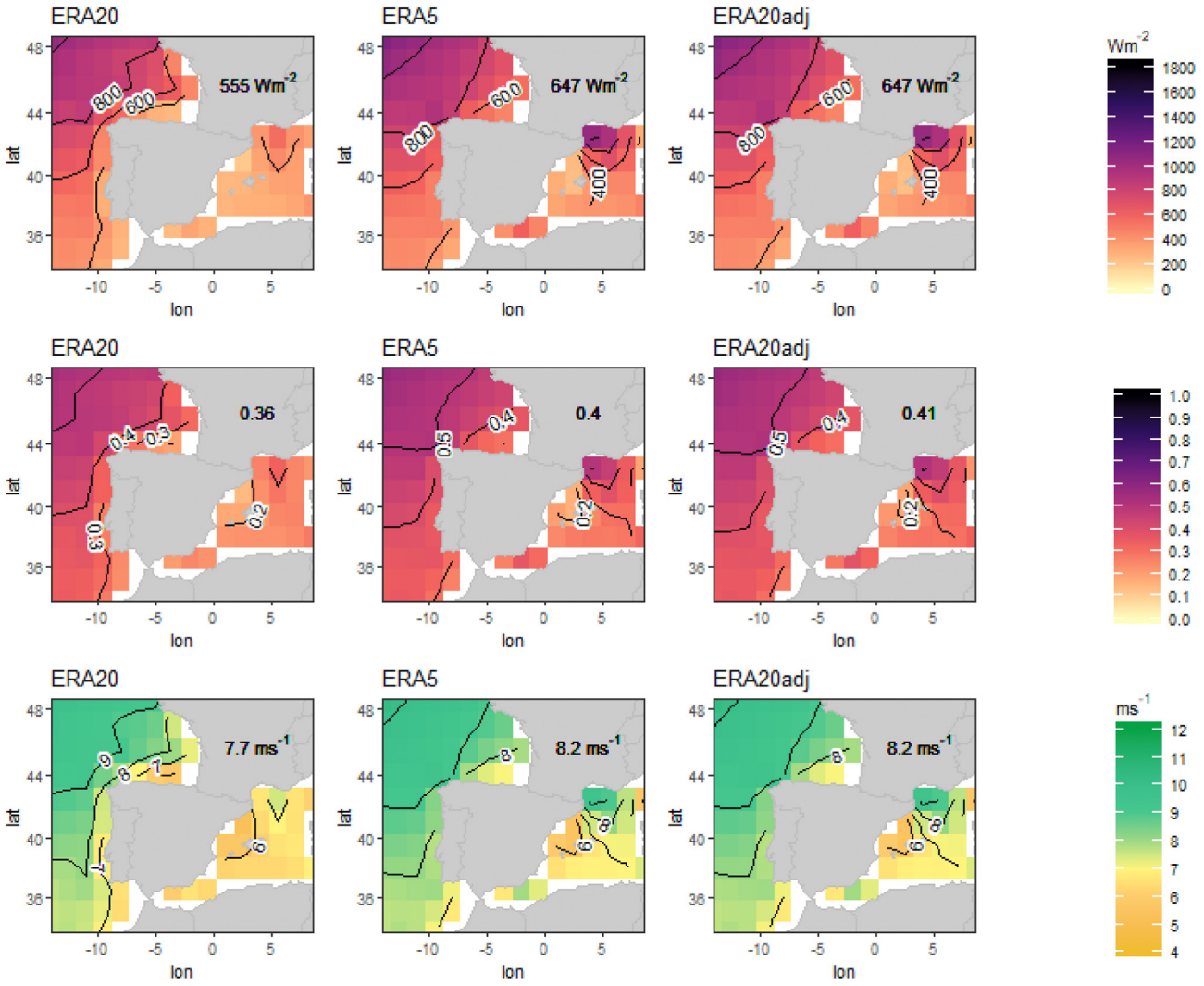

Fig. 2. Mean values of WPD (top), CF (middle), and WS (bottom) for ERA20, ERA5, and ERA20adj in the period 1979–2010, the numerical values written over land correspond to the areal mean WPD and CF.

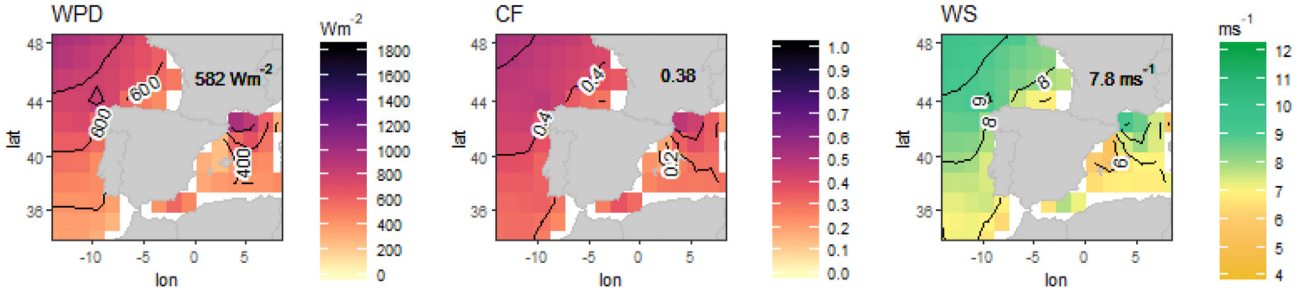

Fig. 3. Mean WPD (left), CF (middle), and WS (right) from ERA20adj in the period 1900–2010, 90 m above the sea surface.

depending on the season (Fig. 5). The values of both WPD and CF are above the mean in winter and below it in summer across the entire study area. In the regions with the highest mean values across all periods, that is, in the NW of the IP and the Gulf of Lyon, differences between winter and summer are ±400 Wm^{-2}, ±0.15, and ±1.7 ms^{-1} for WPD, CF, and WS, respectively.

3.3. Temporal and spatial trends

The decadal trends over the period 1900–2009 were also calculated and derived from the monthly data corresponding to ERA20Adj at each grid point. For graphical representation purposes, the decades have been defined as follows: 1900–1909, 1910–1919, … and 2000–2009. Thus, a total of 11 decades were considered.

The box plot in Fig. 6 was generated using the monthly

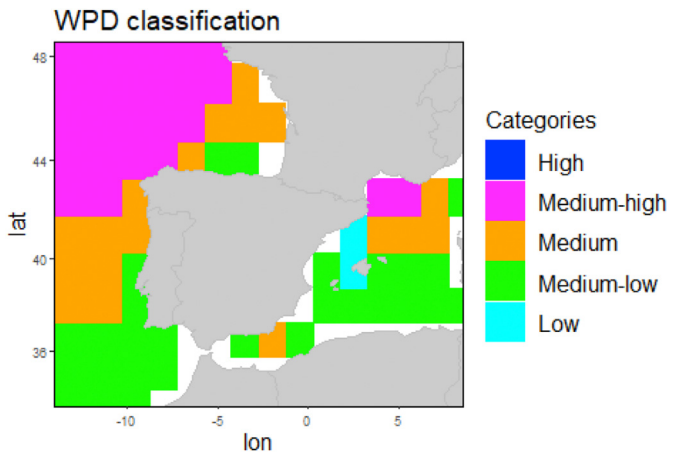

Fig. 4. Classic wind energy classification at a height of 90 m (Table 2).

anomalies. In the figure, a positive trend over the decades in the medians of WPD, CF, and WS can be observed. Specifically, WPD has a positive trend of 13.32 $Wm^{-2}decade^{-1}$ (95% confidence interval from 12.24 to 14.57 $Wm^{-2}decade^{-1}$), calculated using the Theil–Sen estimator. Moreover, as shown in Table 3, the median in each decade is higher than that in the previous one, except in 1920–1929. In the case of CF, there is a trend of 0.72% per decade (95% confidence interval from 0.65% to 0.8%). Additionally, the WS has a positive trend of 0.091 $ms^{-1}decade^{-1}$ (95% confidence interval from 0.082 to 0.1 $ms^{-1}decade^{-1}$).

To check the temporal and spatial evolution, decadal mean values of WPD, CF, and WS were calculated. Fig. 7 shows the maps of the first (1900–1909), sixth (1950–1959), and the last decade (2000–2009) of the study period. It should be noted (Fig. 7) that areas with greater intensity increase over the decades. To find out which areas have the greatest increase, the maps in Fig. 8 show the slopes of the regression lines calculated using the robust Theil–Sein estimator. Grid cells are shaded if the decadal trends are different from zero at the confidence level of 0.95.

To allow a more detailed analysis of the trends across the study area, on one hand, the slopes of the decadal trends at each grid point obtained using the Theil-Sen method [36,37] have been plotted. On the other hand, the mean values of each variable from the first (1900–1909), middle (1950–1959), and last (2000–2009) decades have been plotted.

The slope of the WPD trend is positive and significant across the

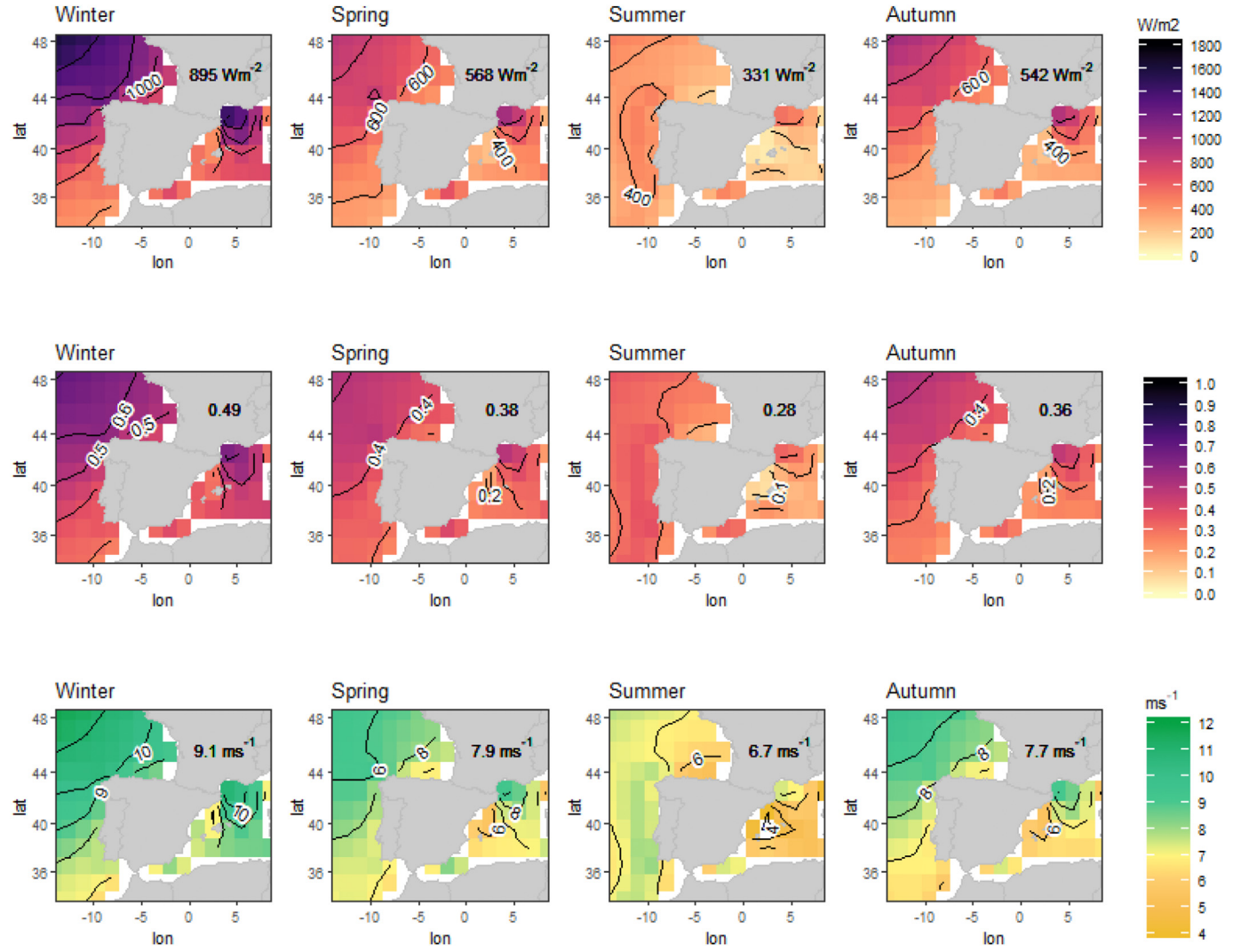

Fig. 5. Seasonal mean values of WPD, CF, and WS by season, in the top, middle, and bottom rows, respectively, from ERA20adj in the period 1900–2010, 90 m above the sea surface.

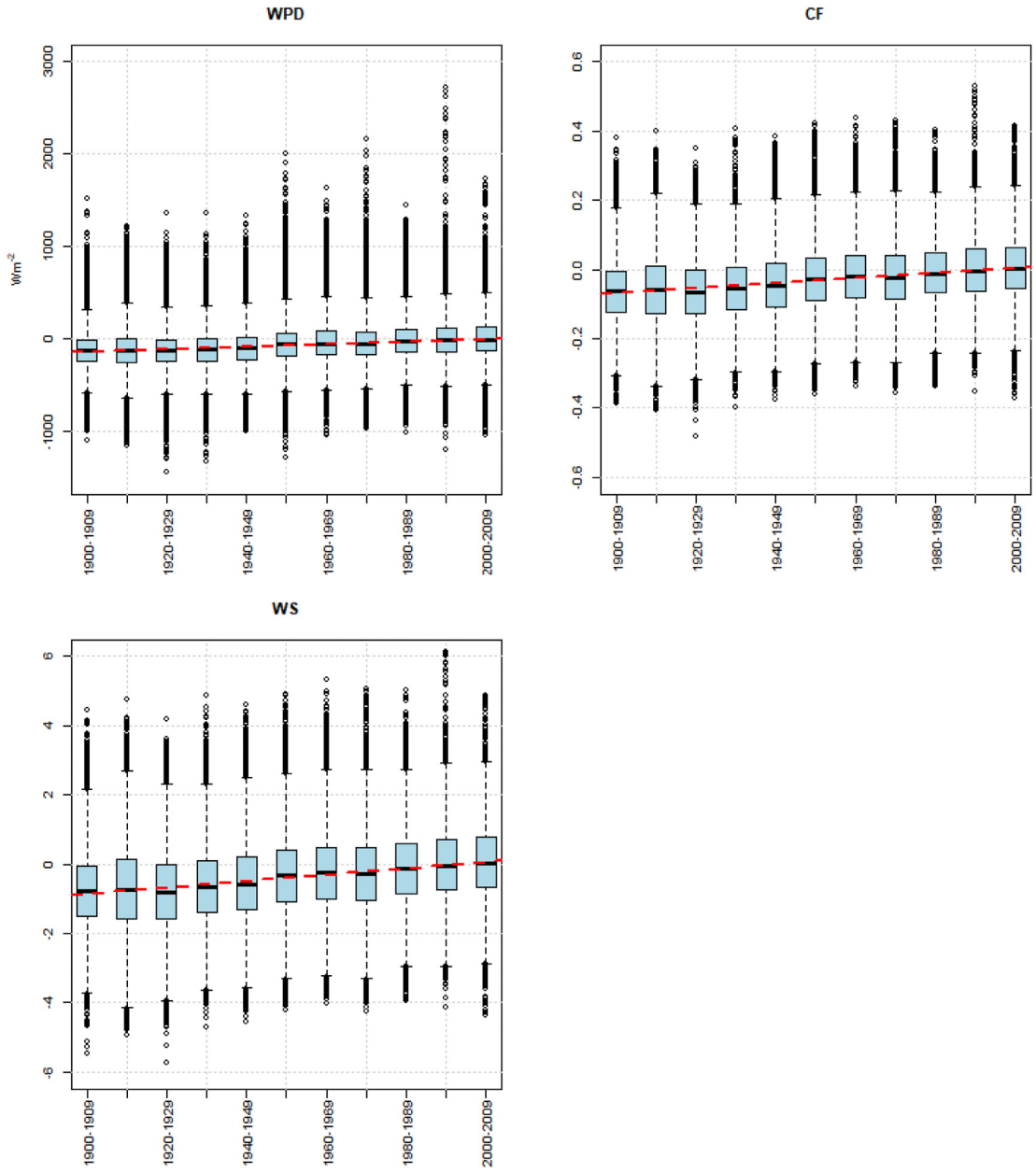

Fig. 6. Decadal box plot of monthly anomalies in WPD, CF, and WS in the period 1900–2009 from ERA20adj. The red dashed line shows the Theil–Sen estimator of the median values. (For interpretation of the references to colour in this figure legend, the reader is referred to the Web version of this article.)

Table 3
Decadal statistics for the monthly anomalies in WPD in the period 1900–2009.

(Wm^{-2})	Min	P_{25}	P_{50}	P_{75}	Max
1900–1909	−1100.12	−248.11	−132.65	−20.3	1521.68
1910–1919	−1160.29	−259.33	−121.74	−1.17	1217
1920–1929	−1437.48	−246.58	−128.05	−13.25	1353.85
1930–1939	−1327.37	−240.27	−118.38	−2.45	1355.39
1910–1949	−995.4	−231.92	−104.76	15.99	1328.39
1950–1959	−1289.49	−191.61	−62.18	59.89	1995.25
1960–1969	−1047.57	−174.57	−55.43	79.3	1632.15
1970–1979	−968.11	−176.45	−53.15	70.75	2153.63
1980–1989	−1021.41	−146.86	−33.66	93.7	1438.84
1990–1999	−1197.34	−136.85	−19.61	111.63	2718.13
2000–2009	−1042.76	−127.79	−12.17	122.75	1727.58

Statistical values indicated as: Min = minimum; P_{25} = 25th percentile; P_{50} = 50th percentile; P_{75} = 75th percentile; and max = maximum.

entire study area (Fig. 8), and is stronger in the Atlantic zone and the Gulf of Lyon, and much weaker around the Balearic Islands. The point with the steepest slope is at the north-western point of the study area (14 °W, 48.5 °N), with a slope of 27.03 $Wm^{-2}decade^{-1}$. The grid point in the Gulf of Lyon (5.5 °E, 42.5 °N) also shows a notably steep slope of 23.81 $Wm^{-2}decade^{-1}$. Further, the mean slope for the entire study area is 15.86 $Wm^{-2}decade^{-1}$, which over the 11 decades, could amount to 174 Wm^{-2}. A similar pattern is observed in the case of CF and WS, namely, a trend that is positive and significant across the study area, which is strongest in the Atlantic and weakest near the Balearic Islands. The mean slopes for CF and WS in the study area are 0.008 $decade^{-1}$ and 0.091 ms^{-1} $decade^{-1}$, which across the 11 decades would be 0.088, and 1 ms^{-1}, respectively.

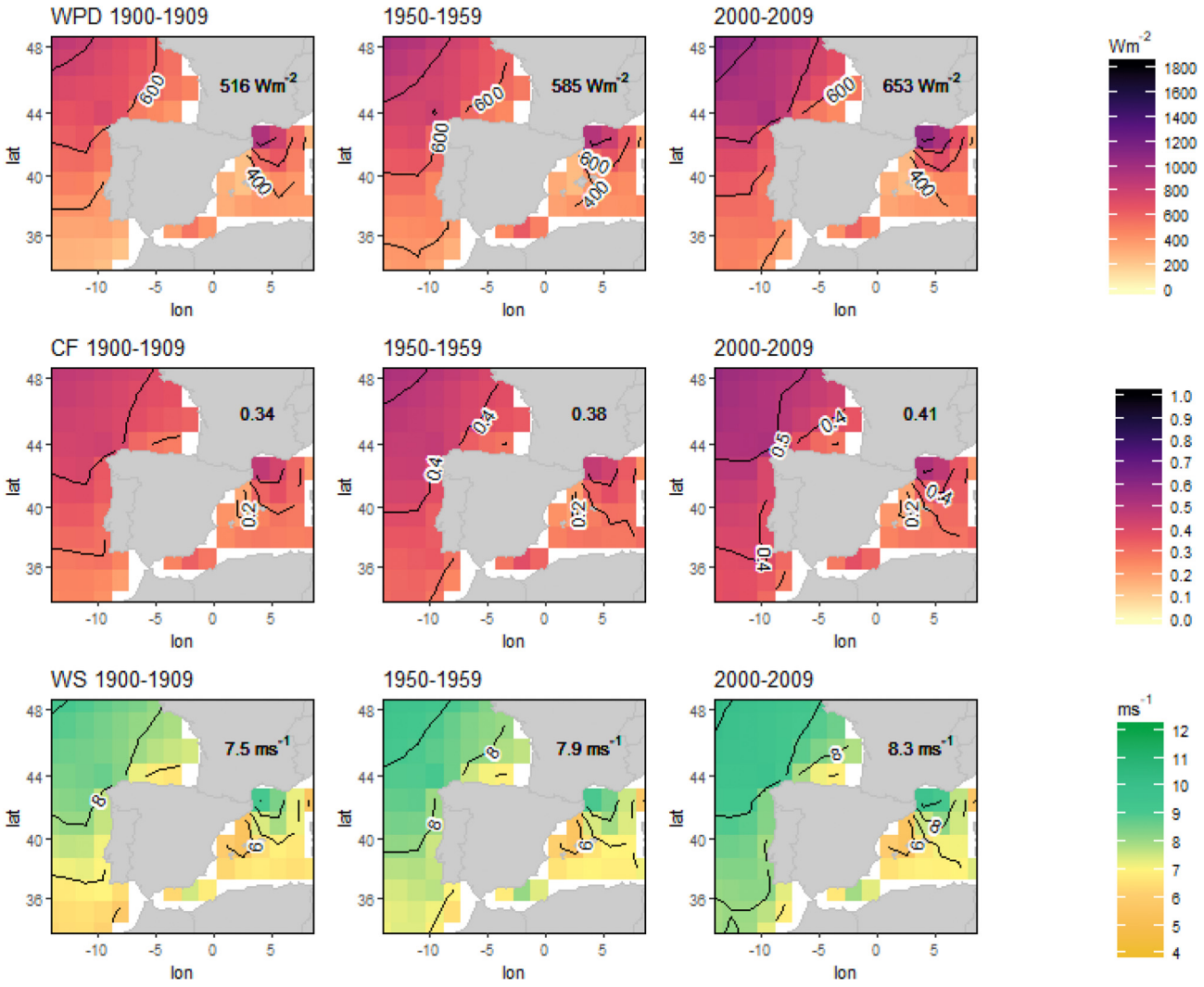

Fig. 7. Mean WPD (left), CF (middle), and WS (right) from ERA20adj for the decades 1900–1909, 1950–1959, and 2000–2009.

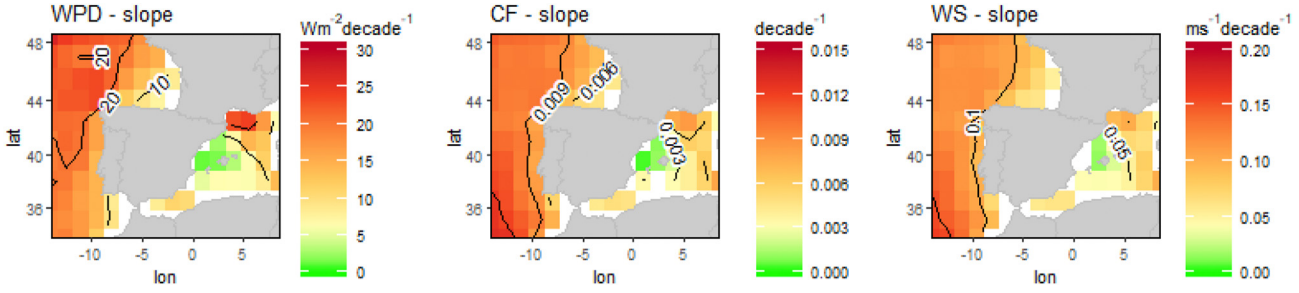

Fig. 8. Map of the decadal trends in WPD, CF, and WS for 1900–2010 obtained using monthly anomalies calculated using ERA20adj data.

4. Discussion

During the period of overlap between ERA20 and ERA5 (1979–2010), it can be seen that the ERA20 reanalysis data underestimates ERA5 for the three target variables WPD, CF, and WS (Fig. 2). Furthermore, as shown by the bias between reanalyses in Fig. 2, the greatest differences are found mainly at points close to the coast, with the largest error in the Gulf of Lyon, a highly energetic area. This is to be expected because the closest grid points to the coast show the greatest variability in topography and present small-scale atmospheric phenomena such as breezes that coarse-resolution models are not able to properly characterise [18].

The areas with the greatest wind potential are located in the northwest of the study area and the Gulf of Lyon with WPD and CF values above 600 Wm^{-2} and 0.4, respectively (Fig. 3). In addition, the area around Cabo de Gata exhibits a high potential, with values of 590 Wm^{-2} and 0.37, respectively. As shown below, these results are in line with previous studies that highlight the same areas as

having the greatest wind energy potential. Furthermore, the results of two studies [63,64] that used ERA5 data to validate the methodology correlated well with those in the present study. The first one [63] focused on Portuguese waters as simulated with the WRF model. It highlighted the north of Portugal, near the coast, as the region with the highest WPD values (909 Wm^{-2}). Using the methodology explained in subsection '2.2.1 Calculation of WS, WPD, and CF' but with the conditions of Campos et al. [63] (using ERA5 without adjusting air density and at a height of 10 m), a WPD of 884 Wm^{-2} was obtained for the same area (point 10 °W, 41 °N). This value is somewhat lower in the current study, probably due to the finer spatial resolution of WRF (0.081° × 0.097°) better representing the characteristics of areas close to the shore. Using the WRF model, Salvador et al. [64] analysed the area around Galicia and found the highest WPD values in the northwestern zone from Cape Finisterre to Cape Ortegal. Specifically, in A Coruña, the WPD reached 1000 Wm^{-2} at a height of 120 m. ERA5 yielded almost identical results, namely, 1001 Wm^{-2} under the same conditions. Another study based on WRF highlighted the potential of A Coruña in the Galician coasts [25] (from 14° to 5 °W and 35° −45° N) with a mean CF of 29–48%. Despite the great differences between the studies, a CF of 35–54% was found in this study in the same domain. Again, the results are notably similar, thus confirming the validity of this study.

Similar studies have also been carried out extensively in the Mediterranean Sea. Ulazia et al. [65] indicated that the Gulf of Lyon had notable potential, with a high CF of 0.46, compared to Menorca, with a considerably lower mean CF (0.3) and a decreasing trend towards the east Mediterranean [14]. Along similar lines, despite differences in the conditions, CFs of 0.46 for the Gulf of Lyon (5.5 °E, 42.5 °N) and 0.27 for the area around Menorca (4 °E, 39.5 °N) were obtained in this study. Based on satellite data, Sukissian et al. [24] also concluded that the Gulf of Lyon (5.5 °E, 42.5 °N) is a candidate for wind farms and highlighted the Cabo de Gata for its relatively high WPD.

To the best of the authors' knowledge, this study is the first to analyse, in depth, the trends and behaviour of WPD, CF, and WS throughout the 20th century around the IP. Analysis of the decadal median trends indicates significant positive trends during 1900–2010. This result is present for all grid points across the study area. Regarding the study variables, the mean WPD and CF values obtained were 15.86 $Wm^{-2}decade^{-1}$ and 0.008 $decade^{-1}$, respectively. Likewise, for peak values, the strongest trends were found in the Atlantic and Gulf of Lyon. In contrast, Cabo de Gata does not stand out, compared to the results for surrounding areas, as has been found previously. The results of this study also show positive trends for WS (0.091 $ms^{-1}decade^{-1}$), in line with recently published studies analysing offshore WS during the 20th century [37,38]. Meucci et al. [37] proved that ERA20 reanalyses present positive trends of WS at a height of 10 m in the Northern Hemisphere, exceeding 0.18 $ms^{-1}decade^{-1}$. However, as per Young et al. [38] 10 m WS satellite data (1985–2018) indicated a significant growth in the Atlantic North zone of 0.1 $ms^{-1}decade^{-1}$, and no clear trend was present in the Gulf of Lyon and Bay of Biscay. Compared with the results obtained in Fig. 6, growth during 1990–1999 and 2000–2009 tended to stabilize. There is no available information for 2010–2019.

Understanding the past evolution of WPD and CF during the last century can be helpful to put into context the estimations for climate change-driven future trends described in other studies. Rusu et al. [30], analysed 30 years of historical data (1976–2005) for the Mediterranean Sea, and found a slight increase in the yearly mean of approximately 8 $Wm^{-2}decade^{-1}$. In contrast, the projections for the period 2021–2050, under a moderate scenario (RCP 4.5), indicated a reduction in wind energy (approximately 12 $Wm^{-2}decade^{-1}$). The Gulf of Lyon (43.23 °N, 4.77 °E) was also identified as a suitable area for wind energy generation. Instead, Costoya et al. [29] investigated the waters off the west of the IP considering RCP 8.5 and analysed the years 2025–2100 and pointed to a reduction in WPD, except in the northwest corner of the IP where hardly any changes or a slight increase can be expected. Zheng et al. [27] concluded that as per RCPs 2.6 and 4.5, although the number of regions with high offshore wind potential (WPD > 800 Wm^{-2}) will slightly decrease worldwide, the number of zones with WPD > 400 Wm^{-2} will increase by the end of the 21st century, and the coasts of the IP lie in this range. Therefore, although previous studies have forecasted reductions in WPD, the aforementioned authors suggest that there may be more zones with wind energy levels above 400 Wm^{-2}, implying an overall increase in WPD. In relation to this, there is a need for further detailed analysis of future projections seeking to identify when and where decreases or increases in WPD can be expected.

Over the entire study period (1900–2010), the mean increase in CF, in the coastal areas around the IP, was 8.8%. In other words, the CF of a reference NREL 5 MW turbine ($P_R = 5$ MW and $D = 126$ m) would have increased from 34% (the CF mean of the first decade 1900–1909, Fig. 8) to 42.8%. Since annual energy production is proportional to CF [10], this would mean an increase in production of more than 900 MWh. For a floating turbine, such as the NREL 5 MW turbine, the increase in annual energy produced over 11 decades with this magnitude of change would be more than 4000 MWh, although the final production of a wind farm cannot be directly derived from the electricity generated by a single turbine. In addition, the studies available on this topic looking to the future are not conclusive, and it is believed that, due to climate change, WPDs could continue to increase in areas that currently have the highest values around the IP coast [43], although this should be analysed in more detail. Considering trends in the last century, the increase in WPD represents an increase in economic returns of at least 20% for each wind turbine compared with early 20th century production, since the rise from 34% to 42.8% represents in relative terms an increase of more than 20%.

This historical trend is of great interest given the expected increase in offshore wind energy in Europe, and the potential reductions in the price of electricity and CO_2 emissions that may follow in the future. The EU is committed to expanding the renewable energy industry, and the economic feasibility of any wind farm is directly dependent on the WPD. It seems clear that a long-life feasibility study requires dynamic knowledge of the WPD evolution at a given location instead of only a static value. The Spanish and Portuguese National Renewable Energy Action Plans incorporates estimations for offshore installed wind power that are expected to reach 59.53 GW in IP [6,7] by 2030. Furthermore, in recent years, there has been a 4.5 €/MWh reduction in the market price of electricity for every 12.8 TWh block installed, due to the penetration of wind energy into the energy market [66]. It has also been demonstrated that the implementation of tens of GW in a region can reduce CO_2 emissions by almost 70% [67].

Finally, it should be pointed out that the increase in CF observed based on resource availability in recent decades could translate to even greater increases in energy production with technical advancements in the aerodynamic and hydrodynamic design of floating turbines. As more technical advances in the field of deep-sea anchoring systems become feasible, more offshore wind power facilities could be built. This includes the generation of hydrogen or methanol at thousands of kilometres from the coast at far-offshore wind farms with an optimal/maximum WPD [68].

5. Conclusions and future outlook

This study shows that the calibration of ERA20 data by quantile-matching with ERA5 data is appropriate to carry out the analysis of the long-term variability of WPD, CF, and WS in the waters off IP. It is shown that during the overlapping years (1979–2010), ERA5 and ERA20adj are very similar.

Considering the values of three variables (WPD, CF, and WS) over the IP, the Atlantic zone, the Gulf of Lyon, and Cabo de Gata were identified as suitable areas to generate offshore wind energy. It has been also proved that during the 20th century and the first decade of 21st, WPD, CF, and WS increased at a rate of 15.86 $Wm^{-2}decade^{-1}$, 0.008 $decade^{-1}$, and 0.091 $ms^{-1}decade^{-1}$, respectively, which corresponds to a total increase of 174 Wm^{-2}, 0.088, and 1 ms^{-1}, respectively. In this period, the areas that have the greatest increase in WPD are the Atlantic zone and the Gulf of Lyon, while for CF, only the Atlantic zone has a significant increase.

Finally, applying these results to a reference turbine throughout the 20th century, an increase in profits of 20% was estimated. This increase could extend over time, especially considering the result of Zheng et al. [27] who considered that the number of zones with WPD > 400 Wm^{-2} will increase by the end of the 21st century.

In the near future, an ERA5 dataset from 1950 to the present is expected to become available. With the inclusion of 30 more years of current reanalysis data, more robust results could be obtained. Additionally, the complete projections of CMIP6 will soon be available, making it possible to assess potential future wind power. Further projections are needed to improve the estimates of what will happen from now until 2100.

In this study, ERA20 reanalysis data from the 20th century (herein ERA20) were used, but this analysis could also be carried out using other atmospheric reanalyses covering the 20th century, such as the NOAA's 20CR. This could be interesting, as previous studies comparing the 20th century reanalyses from NOAA with those from the ECMWF have demonstrated differences [42,69].

Credit author statement

SCM: Methodology, Software, Visualisation, Writing – original draft. GIB: Methodology, Supervision, Writing – review & editing, Project administration JS: Methodology, Supervision, Writing – review & editing, Funding acquisition AU: Methodology, Supervision, Writing – review & editing.

Declaration of competing interest

The authors declare that they have no known competing financial interests or personal relationships that could have appeared to influence the work reported in this paper.

Acknowledgments

This work was financially supported by the Spanish Government through the MINECO project CGL2016-76561-R (MINECO/ERDF, UE) and the University of the Basque Country (UPV/EHU, GIU 17/002). Reanalysis data were downloaded at no cost from the ECMWF. All calculations and plots were carried out in the R framework [70].

References

[1] Liu J-L, Ma C-Q, Ren Y-S, Zhao X-W. Do real output and renewable energy consumption BRICS countries. Energies 2020;13.
[2] Murdock HE, Gibb D, André T, Appavou F, Brown A, Epp B. Renewables 2019 global Status report, 8; 2019. https://doi.org/10.3390/resources8030139.
[3] Papież M, Śmiech S, Frodyma K. Factors affecting the efficiency of wind power in the European Union countries. Energy Pol 2019;132:965–77. https://doi.org/10.1016/j.enpol.2019.06.036.
[4] International renewable energy Agency. IRENA; 1981. https://www.irena.org/. [Accessed 5 June 2020].
[5] European Commission. Renowable energy Onshore and offshore wind. 2019. https://ec.europa.eu/energy/topics/renewable-energy/onshore-and-offshore-wind_en. [Accessed 5 June 2020].
[6] Gobierno de España. Borrador Actualizado del Plan Nacional Integrado de Energía y Clima 2021-2030. 2020. p. 1–8.
[7] República Portuguesa. Plano Nacional Integrado Energia e Clima 2021-2030. 2018. p. 1–106.
[8] European Commission. The European green deal. 2019. https://ec.europa.eu/info/strategy/priorities-2019-2024/european-green-deal_en. [Accessed 5 June 2020].
[9] European Commission. the North seas energy Cooperation. 2020. https://ec.europa.eu/energy/topics/infrastructure/high-level-groups/north-seas-energy-cooperation_en. [Accessed 5 June 2020].
[10] Manwell JF, McGowan JG, Rogers AL. Wind energy explained: theory, design and application. Wiley; 2010.
[11] Masters GM. Renewable and efficient electric power systems. John Wiley & Sons; 2013.
[12] Komusanac I, Fraile D, Brindley G, Walsh C, Pineda I. Wind energy in Europe in 2018. Trends Stat 2019:32.
[13] Smith AZ. Energy numbers 2020. https://energynumbers.info/uk-offshore-wind-capacity-factors. [Accessed 5 June 2020].
[14] Ibarra-Berastegi G, Ulazia A, Saénz J, González-Rojí SJ. Evaluation of Lebanon's offshore-wind-energy potential. J Mar Sci Eng 2019;7:1–13. https://doi.org/10.3390/jmse7100361.
[15] Ulazia A, Nafarrate A, Ibarra-Berastegi G, Sáenz J, Carreno-Madinabeitia S. The consequences of air density variations over northeastern Scotland for offshore wind energy potential. Energies 2019;12. https://doi.org/10.3390/en12132635.
[16] Ulazia A, Sáenz J, Ibarra-Berastegi G, González-Rojí SJ, Carreno-Madinabeitia S. Global estimations of wind energy potential considering seasonal air density changes. Energy 2019;187:115938. https://doi.org/10.1016/j.energy.2019.115938.
[17] Ulazia A, Ibarra-Berastegi G, Sáenz J, Carreno-Madinabeitia S, González-Rojí SJ. Seasonal correction of offshore wind energy potential due to air density: case of the Iberian Peninsula. Sustain Times 2019;11. https://doi.org/10.3390/su11133648.
[18] Elsner P. Continental-scale assessment of the African offshore wind energy potential: spatial analysis of an under-appreciated renewable energy resource. Renew Sustain Energy Rev 2019;104:394–407. https://doi.org/10.1016/j.rser.2019.01.034.
[19] NOAA.. Blended Sea winds 2020. https://www.ncdc.noaa.gov/data-access/marineocean-data/blended-global/blended-sea-winds. [Accessed 18 March 2020].
[20] Rueda-Bayona JG, Guzmán A, Eras JJC, Silva-Casarín R, Bastidas-Arteaga E, Horrillo-Caraballo J. Renewables energies in Colombia and the opportunity for the offshore wind technology. J Clean Prod 2019;220:529–43. https://doi.org/10.1016/j.jclepro.2019.02.174.
[21] NOAA. NCEP north American regional reanalysis: NARR 2020. https://www.esrl.noaa.gov/psd/data/gridded/data.narr.html.
[22] Alkhalidi MA, Al-Dabbous SK, Neelamani S, Aldashti HA. Wind energy potential at coastal and offshore locations in the state of Kuwait. Renew Energy 2019;135:529–39. https://doi.org/10.1016/j.renene.2018.12.039.
[23] Hersbach H. The ERA5 atmospheric reanalysis. AGU Fall Meet Abstr 2016;2016. NG33D–01.
[24] Soukissian T, Karathanasi F, Axaopoulos P. Satellite-based offshore wind resource assessment in the Mediterranean Sea. IEEE J Ocean Eng 2017;42:73–86. https://doi.org/10.1109/JOE.2016.2565018.
[25] Salvação N, Guedes Soares C. Wind resource assessment offshore the Atlantic Iberian coast with the WRF model. Energy 2018;145:276–87. https://doi.org/10.1016/j.energy.2017.12.101.
[26] Skamarock WC, Klemp JB, Dudhi J, Gill DO, Barker DM, Duda MG, Powers JG. A Description of the Advanced Research WRF Version 3 (No. NCAR/TN-475+STR). University Corporation for Atmospheric Research 2008. https://doi.org/10.5065/D68S4MVH.
[27] Zheng C, wei, yan Li X, Luo X, Chen X, Qian Y hao, Zhang Z hua, et al. Projection of future global offshore wind energy resources using CMIP data. Atmos-Ocean 2019;57:134–48. https://doi.org/10.1080/07055900.2019.1624497.
[28] Giorgetta MA, Jungclaus J, Reick CH, Legutke S, Bader J, Böttinger M, et al. Climate and carbon cycle changes from 1850 to 2100 in MPI-ESM simulations for the Coupled Model Intercomparison Project phase 5. J Adv Model Earth Syst 2013;5:572–97. https://doi.org/10.1002/jame.20038.
[29] Costoya X, Rocha A, Carvalho D. Using bias-correction to improve future projections of offshore wind energy resource: a case study on the Iberian Peninsula. Appl Energy 2020;262:114562. https://doi.org/10.1016/j.apenergy.2020.114562.
[30] Rusu E, Rusu L. Evaluation of the wind power potential in the European nearshore of the Mediterranean Sea. E3S Web Conf 2019;103:1–6. https://doi.org/10.1051/e3sconf/201910301003.
[31] Consulting JBA. Performance indicators for offshore wind farms in Europe from 1977 to 2100 derived from climate projections. Copernicus Clim Chang Serv 2020. https://doi.org/10.24381/cds.42c6e4dd.
[32] Consulting JBA. Technical Guide : offshore wind farm operations and

maintenance C3S _ 422 _ Lot2 _ Deltares - European Services. 2019.
[33] Penalba M, Ulazia A, Ibarra-Berastegui G, Ringwood J, Sáenz J. Wave energy resource variation off the west coast of Ireland and its impact on realistic wave energy converters' power absorption. Appl Energy 2018;224:205–19. https://doi.org/10.1016/j.apenergy.2018.04.121.
[34] Ulazia A, Penalba M, Rabanal A, Ibarra-Berastegi G, Ringwood J, Sáenz J. Historical evolution of the wave resource and energy production off the chilean coast over the 20th Century. Energies 2018;11. https://doi.org/10.3390/en11092289.
[35] Kim DI, Kwon HH, Han D. Bias correction of daily precipitation over South Korea from the long-term reanalysis using a composite gamma-pareto distribution approach. Nord Hydrol 2019;50:1138–61. https://doi.org/10.2166/nh.2019.127.
[36] Bett PE, Thornton HE, Clark RT. Using the Twentieth Century Reanalysis to assess climate variability for the European wind industry. Theor Appl Climatol 2017;127:61–80. https://doi.org/10.1007/s00704-015-1591-y.
[37] Meucci A, Young IR, Aarnes OJ, Ø Breivik. Comparison of wind speed and wave height trends from twentieth-century models and satellite altimeters. J Clim 2020;33:611–24. https://doi.org/10.1175/JCLI-D-19-0540.1.
[38] Young IR, Ribal A. Multiplatform evaluation of global trends in wind speed and wave height. Science 2019;364:548–52. https://doi.org/10.1126/science.aav9527. 80-.
[39] Jourdier B. Evaluation of ERA5 and other reanalyses to simulate wind power production over France. EMS Annu Meet Abstr 2019;16:2019.
[40] de Assis Tavares LF, Shadman M, de Freitas Assad LP, Silva C, Landau L, Estefen SF. Assessment of the offshore wind technical potential for the Brazilian Southeast and South regions. Energy 2020;196:117097. https://doi.org/10.1016/j.energy.2020.117097.
[41] Olauson J. ERA5: the new champion of wind power modelling? Renew Energy 2018;126:322–31. https://doi.org/10.1016/j.renene.2018.03.056.
[42] Wohland J, Omrani NE, Witthaut D, Keenlyside NS. Inconsistent wind speed trends in current twentieth century reanalyses. J Geophys Res Atmos 2019;124:1931–40. https://doi.org/10.1029/2018JD030083.
[43] Wohland J, Eddine Omrani N, Keenlyside N, Witthaut D. Significant multi-decadal variability in German wind energy generation. Wind Energy Sci 2019;4:515–26. https://doi.org/10.5194/wes-4-515-2019.
[44] Trenberth KE, Olson JG. An evaluation and Intercomparison of global analyses from the national meteorological center and the European Centre for medium range weather forecasts. Bull Am Meteorol Soc 1988;69:1047–57. https://doi.org/10.1175/1520-0477(1988)069<1047:AEAIOG>2.0.CO;2.
[45] Simmons AJ, Jones PD, da Costa Bechtold V, Beljaars ACM, Kållberg PW, Saarinen S, et al. Comparison of trends and low-frequency variability in CRU, ERA-40, and NCEP/NCAR analyses of surface air temperature. J Geophys Res Atmos 2004;109:1–18. https://doi.org/10.1029/2004JD005306.
[46] Sterl A. On the (in)homogeneity of reanalysis products. J Clim 2004;17:3866–73. https://doi.org/10.1175/1520-0442(2004)017<3866:OTIORP>2.0.CO. 2.
[47] Bloomfield HC, Shaffrey LC, Hodges KI, Vidale PL. A critical assessment of the long-term changes in the wintertime surface Arctic Oscillation and Northern Hemisphere storminess in the ERA20C reanalysis. Environ Res Lett 2018;13. https://doi.org/10.1088/1748-9326/aad5c5.
[48] Jonkman J, Butterfield S, Musial W, Scott G. Definition of a 5-MW reference wind turbine for offshore system development. 2009.
[49] Barthelmie RJ, Jensen LE. Evaluation of wind farm efficiency and wind turbine wakes at the Nysted offshore wind farm. Wind Energy 2010;13:573–86. https://doi.org/10.1002/we.408.
[50] Boccard N. Capacity factor of wind power realized values vs. estimates. Energy Pol 2009;37:2679–88. https://doi.org/10.1016/j.enpol.2009.02.046.
[51] Izquierdo S, Montañs C, Dopazo C, Fueyo N. Analysis of CSP plants for the definition of energy policies: the influence on electricity cost of solar multiples, capacity factors and energy storage. Energy Pol 2010;38:6215–21. https://doi.org/10.1016/j.enpol.2010.06.009.
[52] Wang Z, Li Y, Wang K, Huang Z. Environment-adjusted operational performance evaluation of solar photovoltaic power plants: a three stage efficiency analysis. Renew Sustain Energy Rev 2017;76:1153–62. https://doi.org/10.1016/j.rser.2017.03.119.
[53] Cheng HP, Yu MT. Effect of the transmission configuration of wind farms on their capacity factors. Energy Convers Manag 2013;66:326–35. https://doi.org/10.1016/j.enconman.2012.12.011.
[54] Ulazia A, Ibarra-Berastegi G, Sáenz J, Carreno-Madinabeitia S, González-Rojí SJ. Seasonal correction of offshore wind energy potential due to air density: case of the Iberian Peninsula. Sustain Times 2019;11. https://doi.org/10.3390/su11133648. 2014–6.
[55] Ulazia A, Saenz J, Ibarra-Berastegui G. Sensitivity to the use of 3DVAR data assimilation in a mesoscale model for estimating offshore wind energy potential. A case study of the Iberian northern coastline. Appl Energy 2016;180:617–27. https://doi.org/10.1016/j.apenergy.2016.08.033.
[56] Sáenz J, González-Rojí SJ, Carreno-Madinabeitia S, Ibarra-Berastegi G. Analysis of atmospheric thermodynamics using the R package aiRthermo. Comput Geosci 2019;122. https://doi.org/10.1016/j.cageo.2018.10.007.
[57] Yang S, Wang XL, Wild M. Homogenization and trend analysis of the 1958-2016 in situ surface solar radiation records in China. J Clim 2018;31:4529–41. https://doi.org/10.1175/JCLI-D-17-0891.1.
[58] Squintu AA, van der Schrier G, Brugnara Y, Klein Tank A. Homogenization of daily temperature series in the European climate assessment & dataset. Int J Climatol 2019;39:1243–61. https://doi.org/10.1002/joc.5874.
[59] Gudmundsson L, Bremnes JB, Haugen JE, Engen-Skaugen T. Technical Note: downscaling RCM precipitation to the station scale using statistical transformations - a comparison of methods. Hydrol Earth Syst Sci 2012;16:3383–90. https://doi.org/10.5194/hess-16-3383-2012.
[60] Theil H. A rank-invariant method of linear and polynomial regression analysis. In: Proceedings of koninalijke nederlandse akademie van Weinenschatpen; 1950. https://doi.org/10.1007/978-94-011-2546-8 20.
[61] Sen PK. Estimates of the regression coefficient based on Kendall's tau. J Am Stat Assoc 1968;63:1379–89. https://doi.org/10.1080/01621459.1968.10480934.
[62] Troen I, Lundtang Petersen E. European wind atlas - Errata. 1989.
[63] Campos RM, Guedes Soares C. Spatial distribution of offshore wind statistics on the coast of Portugal using Regional Frequency Analysis. Renew Energy 2018;123:806–16. https://doi.org/10.1016/j.renene.2018.02.051.
[64] Salvador S, Costoya X, Sanz-Larruga FJ, Gimeno L. Development of offshore wind power: contrasting optimal wind sites with legal restrictions in Galicia, Spain. Energies 2018;11:2011–20. https://doi.org/10.3390/en11040731.
[65] Ulazia A, Sáenz J, Ibarra-Berastegi G, González-Rojí SJ, Carreno-Madinabeitia S. Using 3DVAR data assimilation to measure offshore wind energy potential at different turbine heights in the West Mediterranean. Appl Energy 2017;208:1232–45. https://doi.org/10.1016/j.apenergy.2017.09.030.
[66] Pereira AJC, Saraiva JT. Long term impact of wind power generation in the Iberian day-ahead electricity market price. Energy 2013;55:1159–71. https://doi.org/10.1016/j.energy.2013.04.018.
[67] Kempton W, Archer CL, Dhanju A, Garvine RW, Jacobson MZ. Large CO2 reductions via offshore wind power matched to inherent storage in energy end-uses. Geophys Res Lett 2007;34. https://doi.org/10.1029/2006GL028016.
[68] Babarit A, Clodic G, Delvoye S, Gilloteaux JC. Exploitation of the far-offshore wind energy resource by fleets of energy ships - Part 1: energy ship design and performance. Wind Energy Sci 2020;5:839–53. https://doi.org/10.5194/wes-5-839-2020.
[69] Befort DJ, Wild S, Kruschke T, Ulbrich U, Leckebusch GC. Different long-term trends of extra-tropical cyclones and windstorms in ERA-20C and NOAA-20CR reanalyses. Atmos Sci Lett 2016;17:586–95. https://doi.org/10.1002/asl.694.
[70] R Core Team. R: A Language and Environment for statistical computing, R Foundation for Statistical Computing, Vienna, Austria. https://www.r-project.org/2020.